EXPERIMENTAL RESULTS ON SHOCK-WAVE/BOUNDARY-LAYER INTERACTION INDUCED BY A MOVABLE WEDGE

Dennis Daub, Sebastian Willems, and Ali Gülhan

DLR, German Aerospace Center, Institute of Aerodynamics and Flow Technology, 51147 Cologne, Germany

ABSTRACT

Experiments on shock-wave/boundary-layer interaction of an impinging shock on a flat panel at Mach numbers of 3 and 4 were conducted in the Trisonic Wind Tunnel (TMK) of the Supersonic and Hypersonic Technologies Department at DLR, Cologne. To obtain high frequency data, the model was equipped with 12 high-speed pressure transducers for measurements at 100 kHz and high-speed schlieren photography was used. The experimental setup is designed for quick rotation of the shock generator allowing testing at different ramp angles during one wind tunnel run. The static pressure distribution and high speed pressure fluctuations in the interaction area were analysed with regard to the spatial and temporal distribution of occurring frequencies. At the beginning of the separation and near the reattachment, a strong increase of low frequency fluctuations of up to 1 kHz was observed, while in the separated area also higher frequencies were excited. These results were compared to the frequencies and flow topology found in the high-speed schlieren videos.

Key words: SWBLI, shock-wave/boundary-layer interaction, shock unsteadiness, turbulent supersonic boundary layer, shock induced separation.

1. INTRODUCTION

Despite decades of research in this area, the unsteady behaviour of shock-wave/boundary-layer interaction is not fully understood, but of great importance for the design of future space launch systems [1, 2, 3, 4], for example for air-breathing engines, overexpanded rocket nozzles or other parts of the vehicle exposed to incoming shocks. It can have a major influence on vehicle performance and reliability, for example with regard to structural fatigue. Furthermore, it is a challenging test case for validation of any simulation of turbulent supersonic compressible flow.

Shock-wave/boundary-layer interaction occurs in supersonic flow when a shock wave imposes an adverse pressure gradient on a boundary layer that leads to boundary layer separation. Due to propagation in the subsonic part of the boundary layer a pressure rise occurs upstream of the nominal impingement point of the shock wave which in turn strongly affects the supersonic part of the flow field. This system usually shows low frequency motion of the flow structure on the order of about 1 kHz, while high frequency fluctuations are also amplified. A thorough description can be found for example in Délery and Dussauge [4]. These phenomena can generally be observed for two different configurations. The interaction can be obtained due to a shock caused by the geometry of the wall, for a example a compression corner, or by an incident shock on a flat panel. In this paper the latter case is considered.

A comprehensive overview of previous work till 2001 is given by Dolling [5, 6]. With regard to the unsteadiness of the shock-wave/boundary-layer interaction Dolling concludes that no comprehensive theory exists to explain the phenomena observed in a great number of experiments and suggests that new experiments with non-intrusive high-speed instrumentation such as CCD cameras or laser-based techniques might in combination with high-speed pressure transducers lead to a better understanding of the unsteady behaviour of the interaction, perhaps accompanied by high-fidelity Large Eddy Simulations (LES). Dussauge et al. [7] compiled results from various experiments to investigate whether there are some common features of the unsteadiness. He shows for example that the frequencies of the shock oscillations are on the same order of magnitude for some cases possibly yielding at least some general trends. A recent experiment on a case with an incident shock wave at $M = 2.1$ was conducted by Humble et al. [8] using Particle Image Velocimetry (PIV). A Direct Numerical Simulation (DNS) of a case with incident shock at $M = 2.25$ was conducted by Pirozzoli and Grasso [3]. They found large-scale low frequency unsteadiness with peaks at discrete frequencies in the interaction zone. A comparison of different Large Eddy Simulations can be found in Touber and Sandham [9]. All cases showed low frequency motion of the flow structure.

The Collaborative Research Center Transregio 40 (SFB-TRR40) of the German Research Foundation (DFG) is concerned with the investigation of fundamental technologies for future space launch systems. The results presented in this paper were obtained as preparation for planned experiments on fluid-structure interaction with a

shock impinging on an elastic panel meant to further the understanding of the complex physical phenomena occurring in such a configuration, namely turbulent compressible flow, flow separation and aeroelasticity, and to serve as a reference case for validation of coupled LES developed within SFB-TRR 40 [10, 11, 12].

2. EXPERIMENTAL SETUP

2.1. Facility

The experiments were conducted in the Trisonic Wind Tunnel (TMK) of the Supersonic and Hypersonic Technologies Department (Esch [13]) at DLR, Cologne. TMK is a blow-down facility with a Mach number range of 0.5 to 4.5. Mach numbers of up to 5.7 are reached by heating the working gas and using an ejector. For transonic flow, a special test section with perforated walls has to be used. The test section has a rectangular cross section of 0.6x0.6 m. The nozzle contour is variable and can be altered during the wind tunnel run. Typical test conditions for the conducted experiments are given in Table 1. The viscosity used for the Reynoldsnumber is calculated using the Sutherland formula with the coefficients as in [14].

Table 1. Typical test conditions

M	p_∞ [kPa]	T_∞ [K]	v_∞ [$\frac{\mathrm{m}}{\mathrm{s}}$]	Re_∞ [$\frac{10^6}{\mathrm{m}}$]
2.5	21.2	126.7	567	37.7
3.0	15.6	97.2	595	49.4
3.5	11.7	83.2	643	55.1
4.0	8.7	64.9	650	70.1

2.2. Model

The model consists of a base plate (Figure 1) in which a panel equipped with sensors (Figure 3) can be mounted, and a rotatable wedge (dimensions see Figure 2). The position of the shaft shown in Figure 2 is x = -108 mm and z = 182.5 mm. The coordinate system is shown in Figure 1 and Figure 3. The movable wedge allowed quick changes of the ramp angle α even during one wind tunnel run. α is defined as the angle between the test panel and the lower side of the wedge as shown in Figure 1. The wedge spans the width of the test section to obtain a 2-dimensional flow field. The leading edge of the base plate is located at x = -220 mm and has a wedge angle of 10° towards the bottom wind tunnel wall (see Figure 1). Boundary layer tripping was applied at the leading edge to obtain a turbulent boundary layer.

2.3. Instrumentation

To measure pressure fluctuations high-speed Kulite pressure transducers were used. Two Kulite XTL-123CEG-

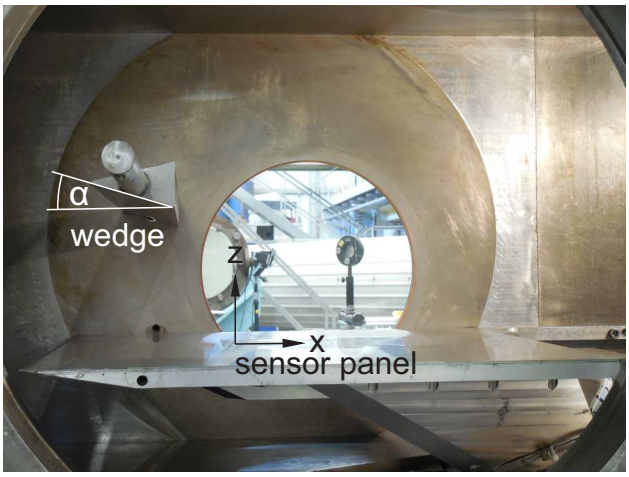

Figure 1. Model

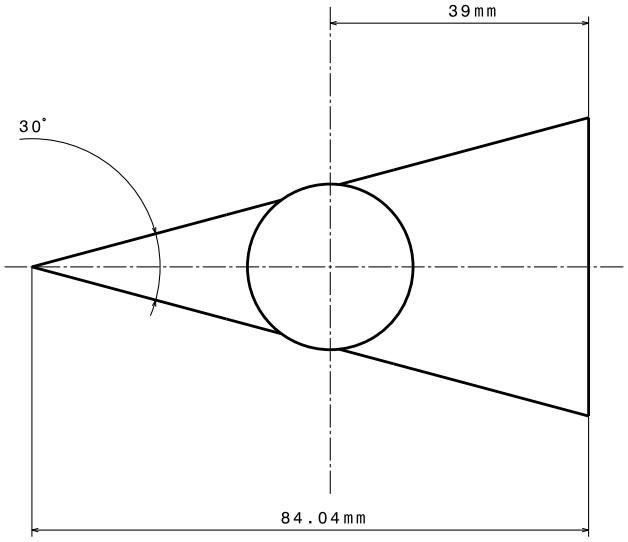

Figure 2. Wedge

190M with a eigenfrequency greater 175 kHz were used upstream and downstream of the test panel and another 10 high speed pressure sensors (Kulite XCQ-062) with a eigenfrequency greater 240 kHz on the test panel. Furthermore 48 Pressure Systems, Inc. (PSI) pressure ports for precise steady state pressure measurement with higher resolution were used. National Instruments 24-bit high speed bridge modules PXIe 4331 were used for data acquisition for the Kulite pressure transducers at a sampling rate of 100 kHz. Figure 3 shows the position of the sensors on the instrumented panel.

A Photron Fastcam SA-X was used for high speed schlieren photography at 20 kHz with a resolution of 1024x200 pixel, and 90 kHz with a resolution of 512x176 pixel to allow high-speed recording of the shock position and flow structure in the separation area. The video analysis was conducted with the OpenCV Library using a Gaussian filter and the Canny edge detection algorithm [15]. This approach is similar to the one described by Es-

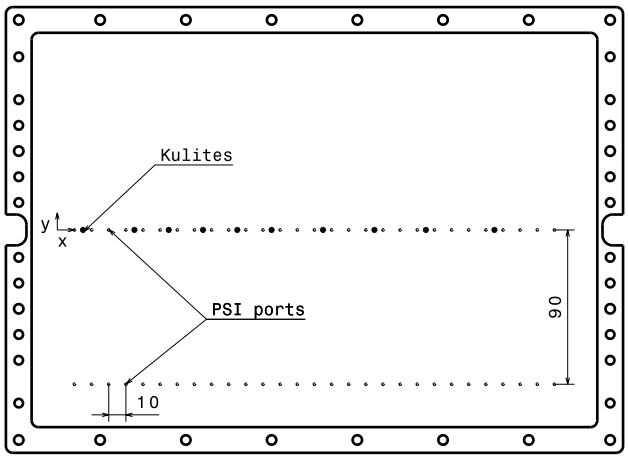

Figure 3. Instrumentation

truch et al. [16]. To compensate the vibration of the optical setup, a software image stabilization algorithm was used.

3. RESULTS AND DISCUSSION

3.1. Incoming Flow

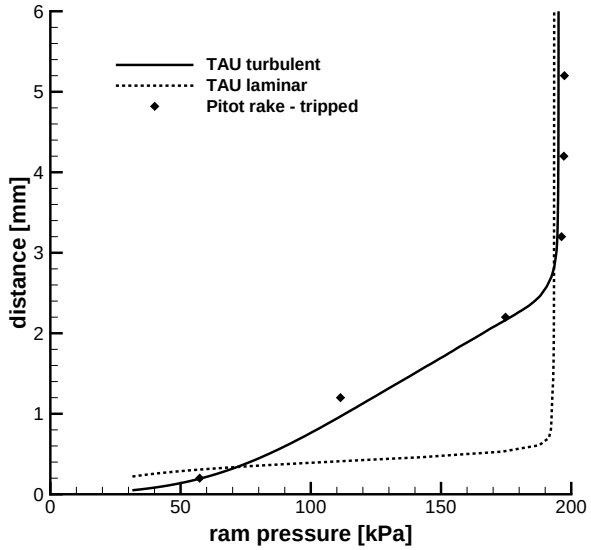

Figure 4. Boundary layer characterisation at $M = 3$ and $x = -70mm$

Laser-2-Focus Velocimetry [17, 18] was used to analyze the incoming flow field. The air flow was seeded with aerosol particles to measure the turbulent intensity and velocity in the incoming flow as also described in Willems et al. [19]. The turbulent intensity was found to be 1.9 % in direction of the flow and 2.3 % in orthogonal direction. The method could not be used to fully resolve the boundary layer. A small pitot rake was used instead and the boundary layer profile shown in Figure 4 was measured and compared to turbulent (Wilcox k-ω turbulence model) and laminar calculation with DLR TAU [20].

3.2. Average Pressure Distribution

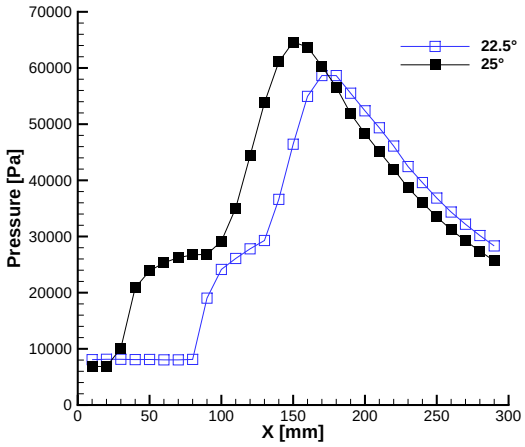

(a) $M = 4$

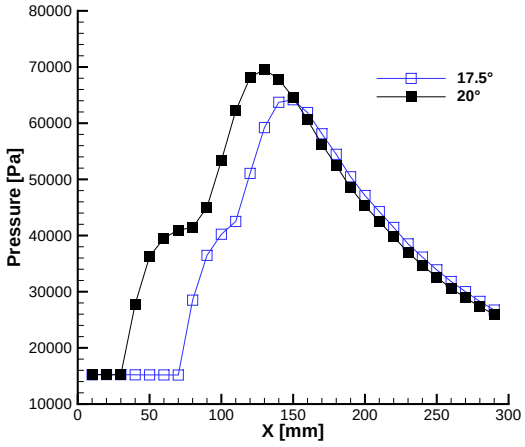

(b) $M = 3$

Figure 5. Static pressure distribution

Figure 5 shows the static pressure distribution on the test panel for $M = 4$ and $M = 3$ at the considered angles α measured with the PSI system. A separation of considerable size is obtained which is suitable for the study of the unsteady phenomena. The data shown were measured on the centerline of the instrumented panel. Further measurements were also conducted at $y = -90\,\mathrm{mm}$ (see Figure 3) to assure two-dimensional behaviour of the flow field. The pressure distributions show good agreement

making for example a LES of a ”slice” of the test panel a reasonable approximation.

3.3. Unsteady Behaviour - Pressure

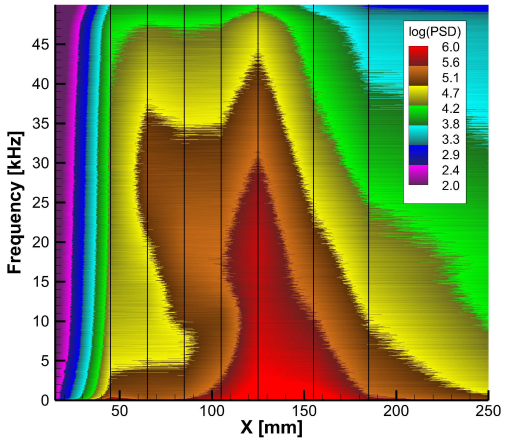

(a) $\alpha = 25°$

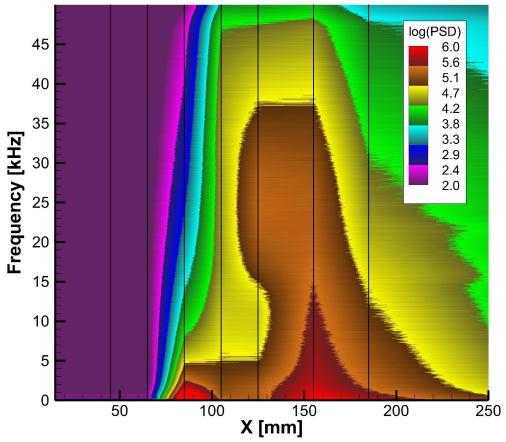

(b) $\alpha = 22.5°$

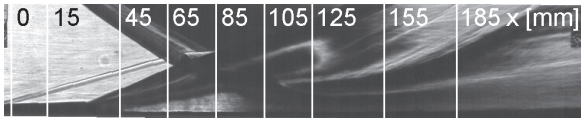

(c) Sensor positions at $\alpha = 25°$

Figure 6. PSD at $M = 4$

The Kulite pressure transducers provide a high-speed pressure signal that was recorded with 100 kHz. Figure 6 and Figure 7 show the spatial distribution of the Power Spectral Density (PSD) of the signal. To obtain the PSD the signal was divided into several blocks with 50 % overlap, the Hann function was applied and the PSD was computed (Welch [21]). Then the blocks were averaged.

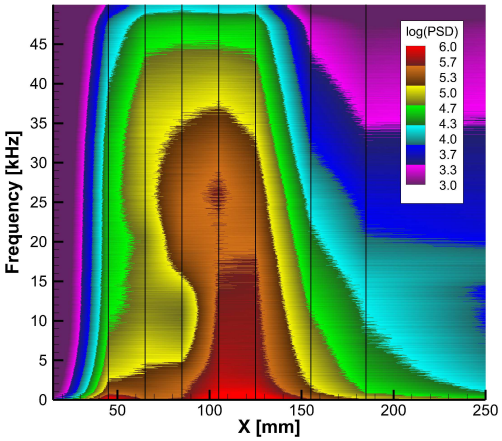

(a) $\alpha = 20°$

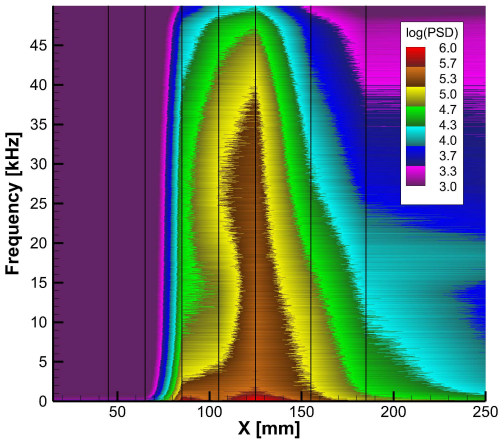

(b) $\alpha = 17.5°$

Figure 7. PSD at $M = 3$

Figure 6(c) shows the sensor positions in the schlieren image at $M = 4$, $\alpha = 25°$. The shock position in this image appears slightly forward of the shock position on the test panel due to side wall effects in the wind tunnel.

It can be seen that for all cases there is a distinct rise in low frequency fluctuations in the vicinity of the separation shock as well as at the reattachment, for Figure 6(a) and Figure 7(a) at about $x = 45\,\mathrm{mm}$, for Figure 6(b) and Figure 7(b) at about $x = 85\,\mathrm{mm}$. These positions correspond to the positions of the initial pressure rise seen in the static pressure distribution in Figure 5. A small change in position is caused by the lower spatial resolution of the high speed measurements compared to the PSI ports. The pressure fluctuations in this area can be attributed to the movement of the separation shock. The resolution of the sensor placement can also lead to a decreased maximum amplitude of the pressure fluctuations as the sensor might not be exactly positioned at the point of maximum pressure fluctuations. Downstream in the

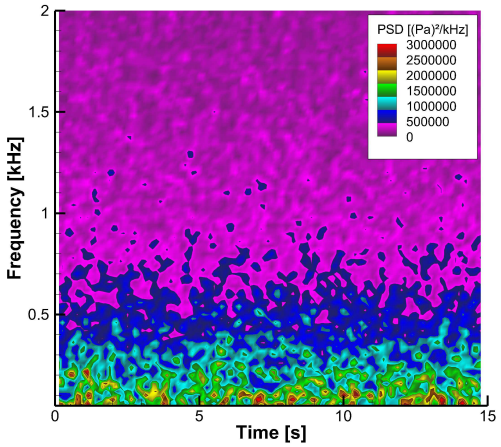

(a) $x = 45mm$

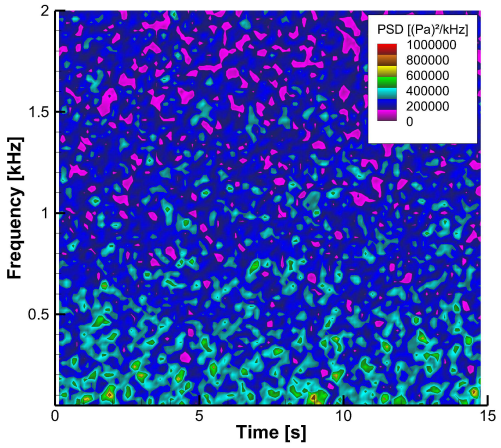

(b) $x = 65mm$

Figure 8. PSD at $M = 3$, $\alpha = 20°$, vicinity of the separation shock

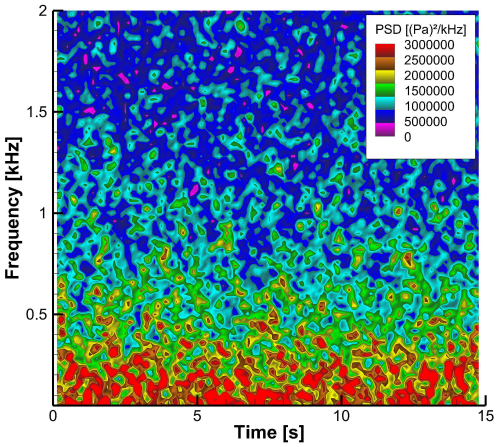

(a) $x = 105mm$

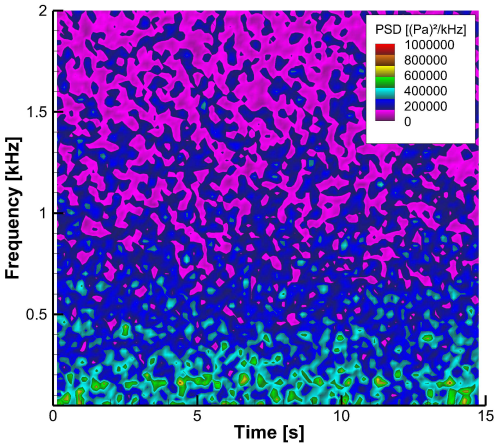

(b) $x = 155mm$

Figure 9. PSD at $M = 3$, $\alpha = 20°$, vicinity of the reattachment

separated area the fluctuation decreases by several orders of magnitude. This position roughly corresponds to the areas with nearly constant pressure seen in Figure 5, for example for $M = 4$ at 25° (Figure 6(a)) in Figure 5(a) from about $x = 60\,\mathrm{mm}$ to $x = 90\,\mathrm{mm}$. A second rise of low frequency fluctuations can be observed in the reattachment area beginning for example at $x = 100\,\mathrm{mm}$ for $M = 4$ at 25° at about the same position as the second rise in pressure occurs in Figure 5(a). Downstream the fluctuations again decrease strongly. For high frequencies the PSD starts to rise in the separated area. For $M = 3$ at $\alpha = 20°$ in Figure 7(a) the rise in power spectral density for high frequencies of up to about 30 kHz starts at about $x = 75\,\mathrm{mm}$ with a peak at about $x = 100\,\mathrm{mm}$. Downstream the power spectral density quickly decreases.

This behaviour is similar to observations made for example for a ramp configuration by Selig et al. [22] and Ringuette et al. [23].

Figure 8 and Figure 9 show the temporal distribution of the Power Spectral Density of the signal at the sensor position $x = 45, 65, 105, 155\,\mathrm{mm}$ for frequencies up to 2 kHz at $M = 3$ at $\alpha = 20°$. Averaged in time the results shown in Figure 8 and Figure 9 can be found in Figure 7(a). As described in the previous paragraph, a strong rise in low frequency pressure fluctuations for frequencies below 1 kHz can be observed in Figure 8(a) at $x = 45\,\mathrm{mm}$, followed by much lower values in Figure 8(b) at $x = 65\,\mathrm{mm}$. Again low frequency fluctuations rise at $x = 105\,\mathrm{mm}$ Figure 9(a) and decrease at $x = 105\,\mathrm{mm}$ Figure 9(b). What is remarkable about this is the great changes of PSD over time. If only a short time span is considered the resulting frequency spectra might look completely different. This should be taken into account for any comparison to short duration DNS or LES calculations.

Special attention should also be given to the pressure sig-

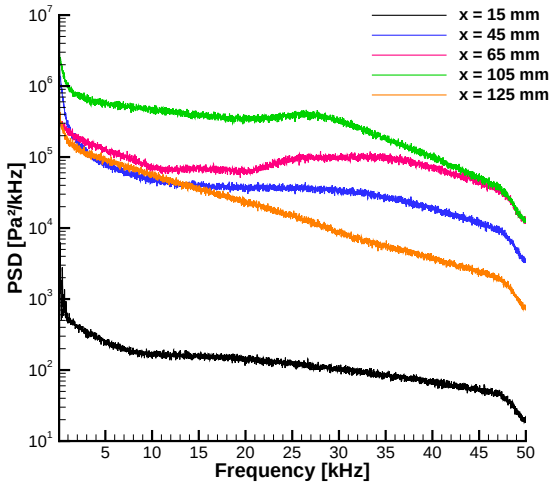

Figure 10. PSD for pressure signals at $M = 3$, $\alpha = 20°$

nal of the sensors upstream of the interaction. Figure 10 shows the PSD at $x = 15\,\mathrm{mm}$ and at the positions shown in Figure 8 and Figure 9. The sensor at $x = 15\,\mathrm{mm}$ is located well ahead of the separation shock. The signal at this position shows no distinct features. The characteristic frequency u_{inf}/δ of the boundary layer ([6]) for about $u = 600\,\mathrm{m/s}$ and $\delta = 4.5\,\mathrm{mm}$ is about 130 kHz which could not be resolved with the sampling rate used.

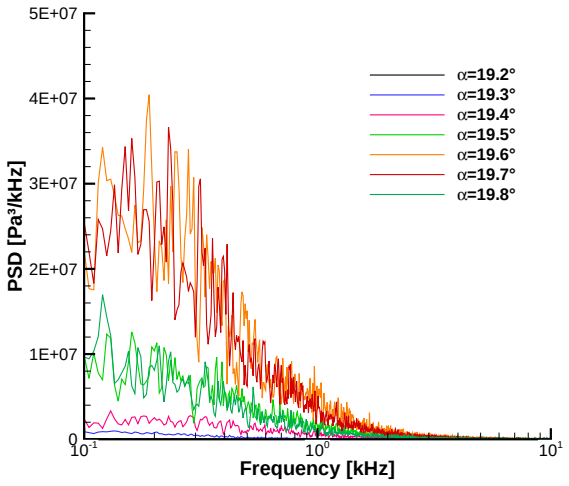

Figure 11. PSD for pressure signals at $x = 45\,\mathrm{mm}$, $M = 3$, $\alpha = 19.2 - 19.8°$

Figure 11 shows the change of the power spectral density for the sensor at $x = 45\,\mathrm{mm}$ during an experiment at $M = 3$ with various wedge angles $\alpha = 19.2° - 19.8°$. This sensor position is closest to the position of the separation shock. The wedge angle is changed in intervals of $0.1°$ to show the effect of the sensor position on the resulting pressure signal. It can be seen that even a small change in shock location leads to a significant difference in the recorded pressure signal. A maximum is reached for $\alpha = 19.6° - 19.7°$. For lower and higher wedge angle the PSD decreases.

3.4. Unsteady Behaviour - Flow Field

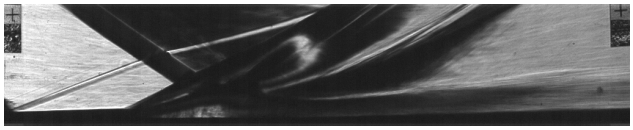

Figure 12. Example of a schlierenimage $M = 3$, $\alpha = 20°$

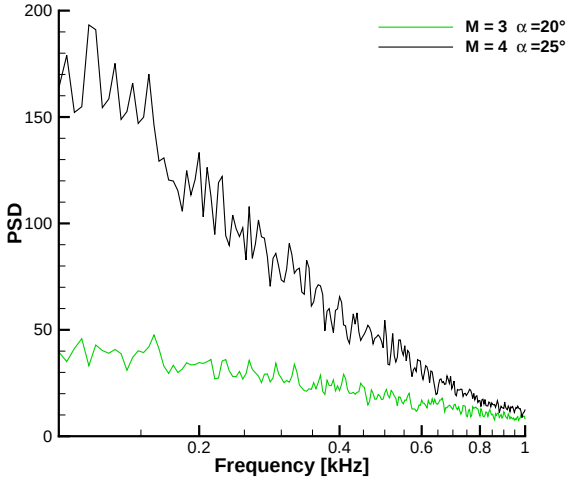

Figure 13. Schlieren at $M = 4$, $\alpha = 25°$ and $M = 3$, $\alpha = 20°$

To gain some insight into the dynamics of the flow field an edge detection algorithm was used to track the position of the separation shock. Figure 12 shows an example of a schlieren image at $M = 3$, $\alpha = 20°$. As previously noted, the shock position seen by the schlieren system does not completely agree with the shock position on the test panel due to side wall effects in the wind tunnel. The results obtained are shown in Figure 13. Especially for the case at $M = 4$, $\alpha = 25°$ a strong rise in low frequency fluctuations can be observed. Again no distinct peaks can be found but a rather broadband oscillation of the shock position. For $M = 3$, $\alpha = 20°$ the changes in shock position are much smaller.

4. CONCLUSION

Experiments on shock-wave/boundary-layer interaction with an impinging shock have been conducted at the Trisonic Wind Tunnel (TMK) of the Supersonic and Hypersonic Technologies Department at DLR, Cologne at $M = 4$ and $M = 3$ at various incident shock angles.

Using high speed pressure transducers some insight into the spatial and temporal distribution of the low frequency unsteadiness of the interaction could be gained. Especially with regard to comparison to relatively short duration LES or DNS calculations the strong temporal variation of the occurring frequencies should be considered. The experiments yielded no discrete frequencies for low frequency movement of the interaction but rather a broadband rise for frequencies below 1 kHz. With regard to the spatial distribution of the unsteady behaviour a strong rise in low frequency pressure fluctuations was observed in the vicinity of the separation shock. Within the separated area these fluctuations reduce by several orders of magnitude followed by a strong rise near the reattachment. In the separated area there is a strong rise in power spectral density of the pressure signals around 25-30 kHz. These results do not by themselves allow a full understanding of the dynamics of the shock-wave/boundary-layer interaction, they yield some insight into the occurring phenomena and provide a data set that numerical simulation or any other kind of model needs to be able to reproduce.

For future experiments it would be desirable to achieve a higher resolution of high speed pressure measurements along the wall and to have improved measurement techniques to obtain data from the flow field such as an improved schlieren system or Particle Image Velocimetry.

ACKNOWLEDGMENTS

This project is financially supported by the German Research Foundation (Deutsche Forschungsgemeinschaft, DFG) within the Collaborative Research Center Transregio 40 (Sonderforschungsbereich Transregio 40). We gratefully acknowledge the help and advice of the technical staff of the Supersonic and Hypersonic Technologies Department in Cologne.

REFERENCES

[1] Robert Schmucker. TUM-LRT Bericht TB-10: Strömungsvorgänge beim Betrieb Überexpandierter Düsen chemischer Raketentriebwerke. Technical report, Technische Universität München - Lehrstuhl für Raumfahrttechnik, München, 1973.

[2] P Pozefsky. Identifying Sonic Fatigue Prone Structures on a Hypersonic Transatmospheric Vehicle (ATV). In *AIAA 12th Aeroacoustics Conference*, San Antonio, TX, 1989. AIAA.

[3] Sergio Pirozzoli and Francesco Grasso. Direct numerical simulation of impinging shock wave/turbulent boundary layer interaction at M=2.25. *Physics of Fluids*, 18(6):065113, 2006. ISSN 10706631. doi: 10.1063/1.2216989. URL http://scitation.aip.org/content/aip/journal/pof2/18/6/10.1063/1.2216989.

[4] Jean Délery and Jean Paul Dussauge. Some physical aspects of shock wave/boundary layer interactions. *Shock Waves*, 19:453–468, 2009. ISSN 09381287. doi: 10.1007/s00193-009-0220-z.

[5] D. S. Dolling. Fluctuating Loads in Shock Wave/Turbulent Boundary Layer Interaction: Tutorial and Update. In *31st Aerospace Sciences Meeting & Exhibit*, Reno, NV, 1993. AIAA. doi: 10.2514/6.1993-284.

[6] D. S. Dolling. Fifty Years of Shock-Wave/Boundary-Layer Interaction Research: What Next? *AIAA Journal*, 39(8):1517–1531, August 2001. ISSN 0001-1452. doi: 10.2514/2.1476. URL http://arc.aiaa.org/doi/abs/10.2514/2.1476.

[7] Jean-Paul Dussauge, Pierre Dupont, and Jean-François Debiève. Unsteadiness in shock wave boundary layer interactions with separation, March 2006. ISSN 12709638. URL http://linkinghub.elsevier.com/retrieve/pii/S1270963805001495.

[8] R. A. Humble, F. Scarano, and B. W. van Oudheusen. Unsteady aspects of an incident shock wave/turbulent boundary layer interaction. *Journal of Fluid Mechanics*, 635:47, September 2009. ISSN 0022-1120. doi: 10.1017/S0022112009007630. URL http://www.journals.cambridge.org/abstract_S0022112009007630.

[9] Emile Touber and Neil D. Sandham. Comparison of three large-eddy simulations of shock-induced turbulent separation bubbles. *Shock Waves*, 19:469–478, 2009. ISSN 09381287. doi: 10.1007/s00193-009-0222-x.

[10] Muzio Grilli, Lin Strobio Chen, Stefan Hickel, Nikolaus Adams, Sebastian Willems, and Ali Gülhan. Experimental and numerical investigation on shockwave/turbulent boundary layer interaction. In *42nd AIAA Fluid Dynamics Conference and Exhibit*, pages 1–15, 2012. URL http://arc.aiaa.org/doi/pdf/10.2514/6.2012-2701.

[11] Muzio Grilli, Stefan Hickel, and Nikolaus Adams. Large-eddy simulation of a supersonic turbulent boundary layer over a compression-expansion ramp. *International Journal of Heat and Fluid Flow*, 42:79–93, August 2013. ISSN 0142727X. doi: 10.1016/j.ijheatfluidflow.2012.12.006. URL http://linkinghub.elsevier.com/retrieve/pii/S0142727X13000052.

[12] Vito Pasquariello, Muzio Grilli, Stefan Hickel, and Nikolaus Adams. Large-eddy simulation of passive shock-wave/boundary-layer interaction control. *International Journal of Heat and Fluid Flow*, 49:116–127, October 2014. ISSN 0142727X. doi: 10.1016/j.ijheatfluidflow.2014.04.005. URL http://linkinghub.elsevier.com/retrieve/pii/S0142727X14000460.

[13] Helmut Esch. Die 0,6-m X 0,6-m-Trisonische Meßstrecke (TMK) der DFVLR in Köln-Porz

(Stand 1986). Technical Report 86-21, DLR, Köln, 1986.

[14] E. H. Hirschel. *Basics of Aerothermodynamics*. Springer-Verlag Berlin Heidelberg New York, 2005. ISBN 3-540-22132-8.

[15] John Canny. A Computational Approach to Edge Detection. *IEEE Transactions on Pattern Analysis and Machine Intelligence*, PAMI-8(6): 679–698, November 1986. ISSN 0162-8828. doi: 10.1109/TPAMI.1986.4767851. URL http://ieeexplore.ieee.org/lpdocs/epic03/wrapper.htm?arnumber=4767851.

[16] D Estruch, N J Lawson, D G MacManus, K P Garry, and J L Stollery. Measurement of shock wave unsteadiness using a high-speed schlieren system and digital image processing. *The Review of scientific instruments*, 79(12):126108, December 2008. ISSN 1089-7623. doi: 10.1063/1.3053361. URL http://www.ncbi.nlm.nih.gov/pubmed/19123599.

[17] Richard Schodl. *Entwicklung des Laser-Zwei-Fokus-Verfahrens für die berührungslose Messung der Strömungsvektoren, insbesondere in Turbomaschinen*. PhD thesis, RWTH Aachen, 1977.

[18] Alain Boutier, Guy Fertin, and Jean Lefevre. Laser Velocimeter for Wind Tunnel Measurements. *IEEE Transactions on Aerospace and Electronic Systems*, AES-14(3):441–455, 1978.

[19] Sebastian Willems, Burkard Esser, and Ali Gülhan. Shock induced fluid structure interaction on a flexible wall in supersonic turbulent flow. In *Progress in Flight Physics - Volume 5*, volume 5, pages 285–308, 2013. doi: 10.1051/eucass/201305.

[20] D. Schwamborn, T. Gerhold, and R. Heinrich. The DLR TAU-Code: Recent Applications in Research and Industry. *Invited Lecture in Proceedings on CD of the European Conference on Computational Fluid Dynamics ECCOMAS CDF 2006*, pages 1–25, 2006.

[21] P. Welch. The use of fast Fourier transform for the estimation of power spectra: A method based on time averaging over short, modified periodograms. *IEEE Transactions on Audio and Electroacoustics*, 15(2):70–73, 1967. ISSN 0018-9278. doi: 10.1109/TAU.1967.1161901.

[22] M. S. Selig, J. Andreopoulos, K. C. Muck, Jean-Paul Dussauge, and a. J. Smits. Turbulence structure in a shock wave/turbulent boundary-layer interaction. *AIAA Journal*, 27(7):862–869, July 1989. ISSN 0001-1452. doi: 10.2514/3.10193. URL http://arc.aiaa.org/doi/abs/10.2514/3.10193.

[23] Matthew J. Ringuette, Patrick Bookey, Christopher Wyckham, and Alexander J. Smits. Experimental Study of a Mach 3 Compression Ramp Interaction at Re{theta} = 2400. *AIAA Journal*, 47(2):373–385, February 2009. ISSN 0001-1452. doi: 10.2514/1.38248. URL http://arc.aiaa.org/doi/abs/10.2514/1.38248.